

Energy and temperature dependencies for electron-induced sputtering from H₂O-ice: Implications for the icy Galilean moons

REBECCA A. CARMACK¹ AND MARK J. LOEFFLER^{1,2}

¹*Department of Astronomy and Planetary Science, Northern Arizona University, Box 6010, Flagstaff, AZ 86011, USA*

²*Center for Materials Interfaces in Research and Applications, Northern Arizona University, Flagstaff, AZ 86011, USA*

ABSTRACT

To better assess the role that electrons play in exosphere production on icy-rich bodies, we measured the total and O₂ sputtering yields from H₂O-ice for electrons with energies between 0.75 and 10 keV and temperatures between 15 and 124.5 K. We find that both total and O₂ yields increase with decreasing energy over our studied range, increase rapidly at temperatures above 60 K, and that the relative amount of H₂O in the sputtered flux decreases quickly with increasing energy. Combining our data with other electron data in literature, we show that the accuracy of a widely used sputtering model can be improved significantly for electrons by adjusting some of the intrinsic parameter values. Applying our results to Europa, we estimate that electrons contribute to the production of the O₂ exosphere equally to all ion types combined. In contrast, sputtering of O₂ from Ganymede and Callisto appears to be dominated by irradiating ions, though electrons still likely contribute a non-negligible amount. While our estimates could be further refined by examining the importance of spatial variations in electron flux, we conclude that, at the very least, electrons seem to be important for exosphere production on icy surfaces and should be included in future modeling efforts.

1. INTRODUCTION

Planetary bodies in our solar system that lack protection from a significant atmosphere are subjected to a number of irradiating particles, such as ions, electrons, photons, and cosmic rays. These particles alter the surface composition and/or structure, as well as eject surface material in a process known as sputtering. The sputtering of surface material can create surface bound exospheres on both rocky (Stern 1999; Wurz et al. 2007, 2010; Gamborino et al. 2019) and icy bodies (Hall et al. 1995; Ip et al. 1997; Cunningham et al. 2015; Ligier et al. 2019; Carnielli et al. 2020; Liuzzo et al. 2020; Plainaki et al. 2020; Paranicas et al. 2022; Carberry Mogan et al. 2023; De Kleer et al. 2023).

Hall et al. (1995) identified an exosphere on Europa containing atomic oxygen and hypothesized that incoming energetic particles cause the dissociation and excitation of molecular O₂ in the atmosphere, which in turn is predicted to be sputtered off Europa's icy surface along with molecular hydrogen and H₂O (Cunningham et al. 2015). Since atomic and molecular hydrogen are

light enough to dissipate into space and H_2O falls back onto the surface, the main component of Europa’s exosphere is oxygen (Johnson et al. 1982, 2009). Similar sputtering processes may occur on Ganymede (Ligier et al. 2019; Paranicas et al. 2022) and Callisto (Cunningham et al. 2015; Carberry Mogan et al. 2023), although the interactions of irradiating particles with those surfaces are more complex.

While both ions and electrons can cause sputtering from icy surfaces, ions have been the main focus of previous experimental (see Baragiola et al. 2003 and Teolis et al. 2017 for a summary) and sputtering/exosphere modeling studies (Famá et al. 2008; Cassidy et al. 2013; Teolis et al. 2017; Addison et al. 2022; Pontoni et al. 2022). The lack of prior attention to electrons is at least partially due to early laboratory data showing that the sputtering yield (Y ; the average number of molecules removed from a target material per incident particle) for a single 100 keV electron (Heide 1984) is 1000 to 10,000 times lower than the sputtering yield for a hydrogen or oxygen ion at similar energies (Shi et al. 1995). However, this difference in sputtering yields may not be that extreme, as the stopping cross section, a parameter which correlates with sputtering, is very low for 100 keV electrons and increases with decreasing energy until it peaks near 0.12 keV (Castillo-Rico et al. 2021). Regardless, electrons contribute $\sim 90\%$ of particles and $\sim 80\%$ of total energy measured near Europa, and smaller but still significant portions of particles/energy measured near Ganymede and Callisto (Cooper 2001). The large flux of electrons near these icy moons could make them important for exosphere production even if electrons are individually less efficient at sputtering than ions.

Previous experiments irradiating H_2O -ice with very low-energy (5 to 100 eV) electrons found that sputtering occurs for energies greater than ~ 10 eV (Sieger et al. 1998; Orlando & Sieger 2003), and that O_2 sputtering yields increase with increasing electron energy between ~ 10 and 100 eV (Sieger et al. 1998; Orlando & Sieger 2003), remain relatively constant at low temperatures (≤ 80 K; Petrik & Kimmel 2005; Davis et al. 2021), and increase with increasing temperature above 80 K (Sieger et al. 1998; Orlando & Sieger 2003; Petrik & Kimmel 2005; Davis et al. 2021).

Three groups have investigated the composition of material sputtered by higher electron energies (Abdulgaliil et al. 2017; Galli et al. 2018; Davis et al. 2021). Both Abdulgaliil et al. (2017) and Galli et al. (2018) detected little to no H_2O sputtered by 0.2 to 10 keV electrons near 100 K, while our group (Davis et al. 2021) determined H_2O dominates material sputtered by 0.5 keV electrons at low temperatures (≤ 60 K) and constitutes $\sim 1/5$ of sputtered molecules at 100 K. Whether these differences between laboratory groups are mainly a consequence of the composition of sputtered material depending on electron energy, as has been observed for ions (Brown et al. 1984; Bar-Nun et al. 1985; Baragiola et al. 2002), or due to other factors is currently unclear.

Quantifying the composition of material sputtered from H_2O -ice as a function of electron energy and temperature is critical to properly model sputtering rates and exosphere production on icy bodies. Recently, we estimated Europa’s global production of O_2 due to electrons by combining our laboratory data (Davis et al. 2021) with the scaled down ion sputtering model from Teolis et al. (2017). We found that electrons could be responsible for sputtering as much or more O_2 as all incoming ions combined (Davis et al. 2021). However, due to a lack of experimental data, we assumed that the composition of sputtered material did not change with electron energy in our calculation.

Thus, here we measure the composition of the sputtering yield as a function of both electron energy and irradiation temperature, using a combination of microbalance gravimetry and mass spectrometry. With our new data, we use Markov chain Monte Carlo methods to determine electron versions of

intrinsic model values that [Teolis et al. \(2017\)](#) determined for ions. Lastly, we use our optimized electron sputtering model to recalculate our previous estimate of the global production rate of O_2 by electrons irradiating Europa ([Davis et al. 2021](#)) and compare our updated model to additional estimates in literature for sputtering of O_2 from Europa, Ganymede, and Callisto, allowing us to better assess the role of electrons in icy satellite exosphere production.

2. EXPERIMENTAL METHODS

We performed all experiments within a stainless steel ultra-high vacuum chamber at a base pressure of $\sim 3 \times 10^{-9}$ Torr ([Meier & Loeffler 2020](#); [Davis et al. 2021](#)). We estimate that the pressure near the sample is 10 to 100 times lower due to a thermal-radiation shield in place around the sample. An Inficon IC6 quartz-crystal microbalance (QCM) with an optically flat gold mirror electrode served as the sample substrate and is mounted onto a rotatable closed-cycle helium cryostat centered inside of the experimental chamber. The cryostat is capable of maintaining temperatures between ~ 10 and 300 K.

We prepared H_2O (HPLC grade) samples in a separate manifold attached to the chamber and grew samples at 100 K at near normal incidence with a deposition rate of $\sim 2 \times 10^{15} \text{ H}_2\text{O cm}^{-2} \text{ s}^{-1}$ to an average column density of $(5.4_{-0.4}^{+1.3}) \times 10^{18} \text{ H}_2\text{O cm}^{-2}$ ($\sim 2 \mu\text{m}$), with the error representing the full range of column densities used in this study. The resulting sample thickness is sufficient to avoid any enhancement in our measured yields for all electron energies studied here ([Meier & Loeffler 2020](#)). We grew fresh films for all electron energies and irradiation temperatures reported here, since sample irradiation history can affect sputtering yields ([Meier & Loeffler 2020](#)). After growth, we changed the sample temperature to the irradiation temperature of interest (between 14 and 125 K). The lower limit ensured we could consistently stabilize the temperature and the higher limit is below the temperature (~ 130 K) where H_2O begins to sublime ([Sack & Baragiola 1993](#)) and out diffusion of radiolytically O_2 produced below the near-surface becomes important ([Teolis et al. 2005](#)).

We irradiated the sample with an EGG-3103C Kimball Physics electron gun at an incident angle of 12.5° with respect to the surface normal with 0.75 to 10 keV electrons. In all experiments, we rastered the beam in an approximately 1×1 cm square, which is larger than the exposed surface of our QCM (~ 8 mm diameter). We measured the electron flux before and after irradiation using a retractable Faraday cup to be $(2.7 \pm 0.8) \times 10^{13} \text{ electrons cm}^{-2} \text{ s}^{-1}$. During irradiation, the flux varied by $\lesssim 2\%$ for all energies except for 10 keV which varied up to $\sim 9\%$. We analyzed any gases present in the chamber, including residual background and material sputtered from the sample during irradiation, using an Ametek Dymaxion Mass Spectrometer (DYMAX-100) aligned 12.5° from the sample normal opposite the electron gun. After each irradiation, we desorbed our ice by turning off the cryostat and allowing the substrate to return to ~ 300 K overnight. In our analysis, we include previous work done by our group in [Davis et al. \(2021\)](#) with 0.5 keV electrons, as they used the same setup and approach as we do here.

3. RESULTS

During irradiation, we see a clear increase in the partial pressure of H_2O , O_2 , and H_2 for each electron energy and temperature studied. However, the background signals for H_2O and H_2 are 1 to 2 orders of magnitude higher than the background for O_2 , and therefore are highly affected by baseline changes. Additionally, the cooled thermal-radiation shield around our sample acts as a potential cold trap for H_2O but is less likely to trap more volatile species like O_2 and H_2 ([Davis et al.](#)

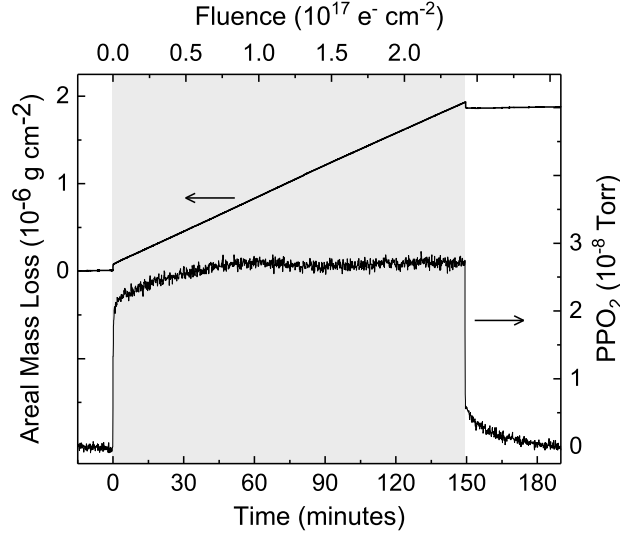


Figure 1. Areal mass loss during irradiation (top) measured by the QCM and O_2 partial pressure (PPO_2 , bottom) measured by the mass spectrometer for a H_2O -ice sample at 115 K irradiated with 1 keV electrons. The highlighted area shows when the electron beam was irradiating the sample.

2021). Because of these barriers to accurately interpreting our partial pressure signals for H_2O and H_2 , we only consider the partial pressure signal for O_2 (PPO_2) in our data analysis.

Figure 1 shows the areal mass loss as monitored by the QCM alongside the baseline subtracted PPO_2 for a sample irradiated with 1 keV electrons at 115 K, with the highlighted area showing when the electron beam was irradiating the sample. When irradiation begins, there is an initial period when the PPO_2 rises until it reaches a peak, after which it levels out at equilibrium for the remainder of the irradiation. In cases where we see a peak ($\gtrsim 115$ K), the fluence required to reach the peak and subsequent equilibrium is energy and temperature dependent. However, all experiments reached equilibrium between fluences of $\sim (0.4 - 3) \times 10^{17}$ electrons cm^{-2} . Generally, we used the equilibrium value to determine the PPO_2 , but in cases where we observed a peak we took the average of the peak and equilibrium values. We incorporated the differences between the peak and equilibrium PPO_2 values into our error. Regardless of irradiation temperature, when the electron gun is blocked the PPO_2 takes time to return to zero. This could be due to any sputtered O_2 remaining in the chamber slowly being pumped out of our system.

Figure 2 shows the total sputtering yield (Y_T ; in terms of the sample’s total mass loss) for 0.5 to 10 keV electrons at temperatures between 14 and 124.5 K. Y_T is approximately constant below 60 K for all energies, although electron energies below ≤ 2 keV show a small ($\lesssim 10\%$) increase in Y_T between 15 and 60 K. For higher energies, we observe a similar trend but cannot say definitively due to increased variation in Y_T . Above 60 K, Y_T clearly increases with temperature. For example, Y_T increases for all energies by a factor of ~ 1.5 between 60 and 100 K, and a factor of 2 to 3 between 60 and 120 K.

In order to determine the composition of sputtered material, we use the same approach described in Davis et al. (2021) for each electron energy studied. We assume the amount of H_2O sputtered from ice for a given electron energy is constant with temperature, previously shown to be true for temperatures $\lesssim 130$ K (Boring et al. 1983; Petrik & Kimmel 2005). Figure 3 (top) shows Y_T versus the PPO_2 for

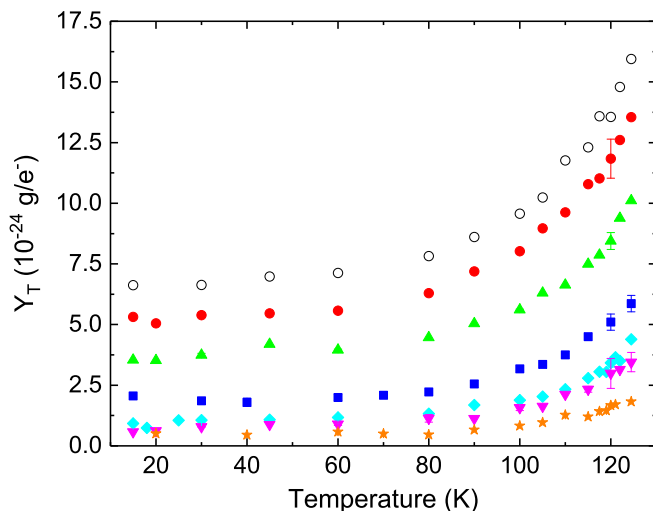


Figure 2. Total sputtering yield (Y_T) versus irradiation temperature for 0.5 (\circ ; from Davis et al. 2021), 0.75 (\bullet), 1 (\blacktriangle), 2 (\blacksquare), 4 (\blacklozenge), 6 (\blacktriangledown), and 10 (\star) keV electrons.

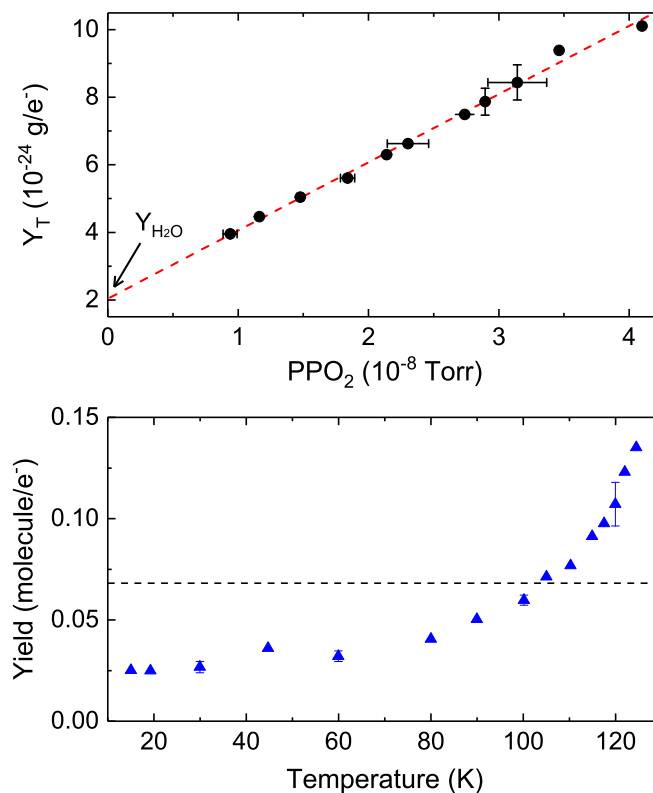


Figure 3. Top: Total sputtering yield (Y_T) versus O_2 partial pressure (PPO_2) for samples irradiated with 1 keV electrons and the resulting linear fit (red dashed line). When the PPO_2 is zero, the only material sputtered is H_2O . Bottom: H_2O (dashed line) and O_2 (\blacktriangle) molecular sputtering yields versus irradiation temperature for 1 keV electrons. The molecular yield of H_2 is presumed to be twice that of O_2 .

Table 1. Summary of Laboratory Sputtering Yields

Energy (keV)	Temperature (K)	Total Yield ^a (10 ⁻²⁴ g/e ⁻)	H ₂ O Yield (10 ⁻²⁴ g/e ⁻)	H ₂ O Yield (H ₂ O/e ⁻)	O ₂ Yield ^{bc} (O ₂ /e ⁻)
0.5 ^d	60	7.13± 0.4	5.1 ± 0.3	0.17 ± 0.01	0.034± 0.01
	100	9.57± 0.2	5.1 ± 0.3	0.17 ± 0.01	0.075± 0.01
	120	13.56± 0.4	5.1 ± 0.3	0.17 ± 0.01	0.141± 0.02
0.75	60	5.57± 0.01	2.8 ± 0.2	0.094± 0.007	0.046± 0.01
	100	8.02± 0.03	2.8 ± 0.2	0.094± 0.007	0.087± 0.02
	120	11.84± 0.81	2.8 ± 0.2	0.094± 0.007	0.151± 0.02
1	60	3.96± 0.03	2.0 ± 0.1	0.068± 0.004	0.032± 0.003
	100	5.61± 0.03	2.0 ± 0.1	0.068± 0.004	0.060± 0.003
	120	8.44± 0.52	2.0 ± 0.1	0.068± 0.004	0.107± 0.010
2	60	1.99± 0.1	0.48± 0.24	0.016± 0.008	0.025± 0.006
	100	3.17± ...	0.48± 0.24	0.016± 0.008	0.045± 0.004
	120	5.10± 0.3	0.48± 0.24	0.016± 0.008	0.077± 0.096
4	60	1.17± 0.04	0.18± 0.45	0.006± 0.015	0.017± 0.008
	100	1.89± 0.04	0.18± 0.45	0.006± 0.015	0.029± 0.008
	120	3.42± 0.17	0.18± 0.45	0.006± 0.015	0.054± 0.011
6 ^e	60	0.90± 0.06	-0.29± 0.3	0.0 ± 0.01	0.015± 0.006
	100	1.58± 0.12	-0.29± 0.3	0.0 ± 0.01	0.026± 0.007
	120	2.99± 0.62	-0.29± 0.3	0.0 ± 0.01	0.050± 0.015
10	60	0.58± 0.20	0.12± 0.22	0.004± 0.007	0.008± 0.007
	100	0.82± ...	0.12± 0.22	0.004± 0.007	0.012± 0.008
	120	1.67± 0.25	0.12± 0.22	0.004± 0.007	0.026± 0.011

^aerror from the spread in values from repeated experiments

^bmolecular yield of H₂ is twice that of O₂ ($Y_{H_2} = 2 * Y_{O_2}$)

^cerror in O₂ estimated from either propagating the error from the repeatability of experiments or from the difference between our measured Y_{O_2} and the linear trend for Y_{O_2} versus S_e for a given temperature (shown in Figure 4 for 60 K), whichever is larger

^dfrom Davis et al. (2021)

^ethe y-intercept of Y_T versus the PPO_2 for 6 keV is negative but zero within error, so we assume the amount of water sputtered is zero

all experiments where we irradiated our sample with 1 keV electrons above 60 K. Each data point is an experiment completed at a different temperature (if a temperature was repeated more than once, the average data point for that temperature is shown). We do not include experiments performed at temperatures below 60 K in the analysis, because baseline variations in the mass spectrometer signal occur more frequently at lower temperatures and because Y_T is ~constant below 60 K. We calculate the sputtering yield of H₂O (Y_{H_2O}) for a given electron energy by extrapolating the PPO_2 to zero

(i.e. the y-intercept in the top of Figure 3), implying no O_2 (or consequentially H_2) is sputtered from the sample. We tested whether the y-intercept was unique for a given electron energy by repeating a suite of experiments under the same conditions (energy, temperatures, etc.) but using a different mass spectrometer multiplier voltage. In those experiments, we find that the data remains linear (although the slope changes) and the y-intercept remains the same.

The difference between Y_T and Y_{H_2O} gives the portion of sputtered material that is comprised of radiolytic products O_2 and H_2 . The sputtering yields for O_2 (Y_{O_2}) and H_2 (Y_{H_2}) are then differentiated from each other by multiplying the sputtered mass of radiolytic products by the mass fraction of O_2 and H_2 in the relation $2 \cdot H_2O \rightarrow O_2 + 2 \cdot H_2$ (Brown et al. 1980b). We show the compositional breakdown of molecules sputtered by 1 keV electrons in Figure 3 (bottom) for each irradiation temperature studied. While we did not measure Y_{H_2} directly, we assume it is twice that of Y_{O_2} (see above).

We apply the same analysis to 0.75, 2, 4, 6, and 10 keV electrons and provide a sampling of representative total mass yields, H_2O mass yields and H_2O and O_2 molecular yields in Table 1 (for the entirety of our data see Table 4 in Appendix A). We find that the composition of sputtered material varies strongly across 0.5 to 10 keV and 60 to 125 K. At low temperatures (≤ 60 K), H_2O makes up as much as 65% of the sputtered flux for 0.5 keV electrons, about 40% for 1 keV electrons, but only comprises about 20% for 2 keV electrons. Above 4 keV, the contribution of H_2O to the sputtered flux is essentially zero within our error. At higher temperatures (>60 K), H_2O yields trend similarly with energy as they do at low temperatures, however the relative contribution of H_2O at each temperature is lower due to the increased production of radiolytic O_2 and H_2 . For instance, at 120 K H_2O makes up about 30% of the sputtered flux at 0.5 keV, about 20% at 1 keV, but drops to about 6% of the flux at 2 keV.

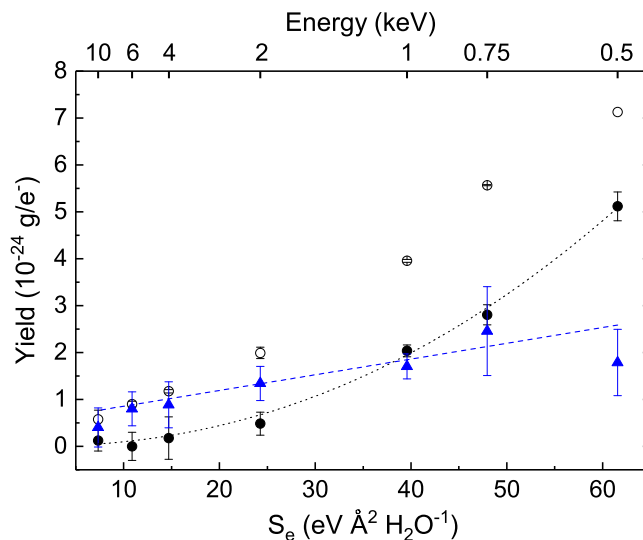


Figure 4. Total (\circ), H_2O (\bullet), and O_2 (\blacktriangle) mass yields of sputtered molecules versus electron stopping cross section (S_e) for all electron energies (0.5 keV from Davis et al. 2021, the rest from this work) at an irradiation temperature of 60 K. We also plot the linear fit to O_2 yields (blue dashed line) and the nearly quadratic fit to H_2O yields (black dotted line). The fit for H_2O is applicable for all temperatures, and follows $y = a(S_e)^n$ where $a = 6.65 \times 10^{-28}$ and $n = 2.17$.

Figure 4 shows the total, H₂O, and O₂ mass yields versus electron stopping cross section (S_e) for irradiation at 60 K. Y_{H_2O} (in g/e⁻, for all temperatures) is nearly quadratic with S_e , and well fit to $y = a(S_e)^n$ where $a=6.65 \times 10^{-28}$ and $n=2.17$. At lower temperatures, the total sputtering yield is superlinearly related to S_e , which is consistent with previous studies (Meier & Loeffler 2020). As temperature increases, the trend of Y_T with S_e becomes more linear, likely because Y_{O_2} (and Y_{H_2}) appear to increase linearly with S_e for all temperatures, though given the error on O₂ yields this is hard to state definitively.

4. COMPARISON TO OTHER EXPERIMENTS

In this study, we expanded on our previous work (Meier & Loeffler 2020; Davis et al. 2021) to investigate the composition of the sputtering yield as a function of irradiation temperature and electron energy. Below, we compare and discuss our results with previous ion and electron work measuring total sputtering yields, as well as studies that have made estimates of the main species sputtered from H₂O-ice.

4.1. Total Yields

Previous work on the sputtering of H₂O-ice with light ions at low temperatures ($\lesssim 80$ K) found Y_T to be proportional to S_e following a superlinear and in some cases quadratic dependence (Brown et al. 1980a,b; Shi et al. 1995; Baragiola et al. 2003). Our group finds a similar superlinear dependence on Y_T with S_e for electron energies between 0.5 and 10 keV irradiating H₂O-ice at lower temperatures (this work, Meier & Loeffler 2020), but the trend progressively becomes more linear with increasing temperature. The dependence of Y_T with S_e ranging from quadratic to linear is likely due to changes in the composition of the sputtered flux (see Section 4.2). In contrast, Galli et al. (2018) found Y_T was independent of S_e between 0.2 and 3 keV for thin films irradiated with electrons at 90 K. We suspect that their observed constancy of Y_T with energy is likely a consequence of using previously irradiated samples, as processed samples can show enhancements in Y_T by a factor of ~ 3 to 6 at 60 K (Meier & Loeffler 2020), which we attribute to the buildup of O₂ beneath the sample’s surface.

At low temperatures (≤ 60 K), we observe a slight ($\lesssim 10\%$) increase in Y_T between 15 and 60 K, which is consistent with previous studies for electrons (Petrik & Kimmel 2005; Davis et al. 2021). For higher temperatures, we find that Y_T increases rapidly above ~ 60 K for all electron energies studied, consistent with our previous work with 0.5 keV electrons (Davis et al. 2021) and with previous ion irradiation studies (Brown et al. 1984; Baragiola et al. 2002, 2003; Famá et al. 2008).

4.2. Composition of the Sputtered Flux

We find that the composition of the sputtered flux depends on both electron energy and irradiation temperature. Changes in the composition of our sputtered flux with electron energy are consistent with previously observed experimental trends for ions, which have shown the composition changes with ion energy and ion type. More specifically, experiments with 1.5 MeV He⁺ found that H₂O makes up $\sim 90\%$ of the sputtered flux at low temperatures (Brown et al. 1984), while only about $\sim 30\%$ is H₂O for 1 to 5 keV H⁺ (Bar-Nun et al. 1985). Variations in composition are also observed with heavier ions: samples irradiated with 1 to 5 keV Ne⁺ found H₂O comprises about 60% of the sputtered flux at 1 keV but only about 30% at 5 keV. Additionally, studies using 100 keV Ar⁺ show that $\sim 75\%$ of the sputtered flux is H₂O (Baragiola et al. 2002).

In addition, we find that H₂O, and possibly also O₂, has a quantifiable dependence on S_e (Figure 4). Our observed quadratic dependence for Y_{H_2O} is consistent with what has been seen for Y_T in

previous studies with fast ions (Brown et al. 1980b; Baragiola et al. 2003). Given that H₂O is the dominant component sputtered by fast ions (Brown et al. 1984), we speculate that the quadratic dependence for Y_{H_2O} observed in our experiments is also a result of excitation pairs overlapping at the surface (Brown et al. 1980b; Baragiola et al. 2003). For O₂, the possible linear relation with S_e suggests that the multiple reactions required to form O₂ from H₂O (Boring et al. 1983; Teolis et al. 2005) may occur from a single electron breaking multiple bonds as it travels into the ice.

We can also compare our results to the two other groups who estimate the composition of flux sputtered from H₂O-ice by ~keV electrons. Abdulgalil et al. (2017) irradiated films coated with islands of C₆H₆ with ~0.25 keV electrons at 112 K. During irradiation, they observed a H₂ signal, a much weaker O signal, but no H₂O signal above the noise level; no measurement of O₂ was reported. They conclude that H₂ and O₂ are the dominant species removed during irradiation, which is inconsistent with our findings that H₂O makes up 45% of our total sputtering yield at 110 K for 0.5 keV electrons. Interestingly, Galli et al. (2018) irradiated several H₂O-ice types (thin films, frost, etc.) with 0.2 to 10 keV electrons at ~90 K and, similar to Abdulgalil et al. (2017), did not see a rise in H₂O above their detection limit while irradiating. They report an average composition between 0.4 and 10 keV for their frost and fine-grained ice samples, estimating the contribution of H₂O to the sputtering yield to be <10%. Although it is unclear what energies were averaged, this upper limit may be in-line with our findings. For instance, H₂O only contributes ~13% for 2 keV electrons at 90 K and subsequently less at energies approaching 10 keV. Using processed H₂O-ice films, as in Galli et al. (2018), may act to suppress the relative contribution of H₂O further, as the total yield can be enhanced temporarily due to the presence of O₂ below the sample's surface (Meier & Loeffler 2020).

Besides the compositional dependence on energy (S_e), we also see a clear increase in the O₂ yield with temperature. For ions, this increase with temperature has been attributed to the ability of radiolytically produced radicals to diffuse and increase production of H₂ and O₂ near the surface (Brown et al. 1980b; Baragiola et al. 2003; Teolis et al. 2009). Our findings support a similar process for electrons, as expected from previous low-energy (~eV) electron irradiation studies showing that Y_{H_2O} remains constant with irradiation temperature (Petrik & Kimmel 2005) while Y_{O_2} is relatively constant (but still increases slightly) below ~60 K and increases rapidly as temperature increases above ~60 K (Petrik & Kimmel 2005; Petrik et al. 2006; Orlando & Sieger 2003).

5. MODELING O₂ SPUTTERING

As noted in the Introduction, between ions and electrons, ions have been the main focus of previous sputtering/exosphere modeling studies (Marconi 2007; Famá et al. 2008; Teolis et al. 2010; Cassidy et al. 2013; Teolis et al. 2017). The most comprehensive model for predicting O₂ sputtering yields for any particle irradiating an icy surface is Teolis et al. (2017) which builds off their work in Teolis et al. (2010).

Teolis et al. (2017) calculates the sputtering yield of O₂ as

$$Y_{O_2}(E, T, \beta) = \frac{\epsilon g_{O_2}^0 x_0}{r_0 \cos \beta} \left[1 - \exp\left(-\frac{r_0 \cos \beta}{x_0}\right) \right] \left[1 + q_0 \exp\left(-\frac{Q}{k_B T}\right) \right], \quad (1)$$

where ϵ is the effective particle energy contributing to sputtering (total energy $E = \epsilon$ for electrons), T is the irradiation temperature, β is the particle's incident angle, $g_{O_2}^0$ is the surface radiolytic yield of O₂ (Y_{O_2}/E when $r_0 \cos \beta \ll x_0$), x_0 is the optimal depth for O₂ production, $r_0 \cos \beta$ is the particle's

range, q_0 is the exponential prefactor for the temperature dependence, k_B is the Boltzmann constant, and Q is the “activation” energy (noted in Teolis et al. 2017 to not have a determined physical significance). Teolis et al. (2017) fit Equation 1 to existing laboratory data for ions and determined intrinsic parameter values for $g_{O_2}^0$, x_0 , q_0 , and Q (listed in Table 2).

In Tribbett & Loeffler (2021), we determined that Equation 1 overestimates O_2 production from ions with ranges $r_0 \cos \beta \gg x_0$ by as much as an order of magnitude and explored how this could be caused by the assumption in Teolis et al. (2017) that energy is deposited uniformly over the ion’s range. Upon further investigation, we noticed a mistake in Teolis et al. (2017) regarding the angle of incidence for data taken by Bar-Nun et al. (1985)¹ for highly penetrating ions, which could also be contributing to the discrepancy between Equation 1 and experimental data. We are hoping to revisit the effects of these corrections in a future study.

5.1. Scaling the Model to Electrons

The model’s predicted O_2 sputtering trends are generally consistent with what has been observed for electrons (see Introduction). Thus, it seems reasonable that first attempts to model electron sputtering simply scale Equation 1, calculated with parameter values derived using ion data, down by a constant factor ($C * Y_{O_2}$) since at the time there was a lack of electron data with which to determine electron specific parameter values. Teolis et al. (2010, 2017) uses a factor of $C=0.29$ to fit $C * Y_{O_2}$ to experimental O_2 yields for low-energy (5 to 30 eV) electrons provided by Petrik, Kavesky, and Kimmel at Pacific Northwest National Laboratory (supplemental Figure S9 in Teolis et al. 2010), although

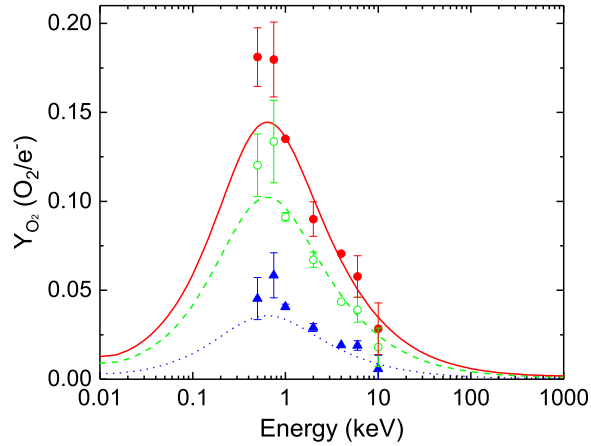


Figure 5. Our group’s experimental data (0.5 keV from Davis et al. 2021, the rest from this work) for irradiation temperatures of 80 K (\blacktriangle), 115 K (\circ) and 124.5 K (\bullet) compared to Equation 1 scaled down by our best-fit scaling factor of 0.12 for 80 K (blue dotted line), 115 K (green dashed line), and 124.5 K (red solid line).

¹ The Bar-Nun et al. (1985) paper states that their angle of incidence is 60° . However, it appears that the ions are incident 60° with respect to the surface and therefore 30° with respect to the surface normal. For our reasoning, compare the text in paragraph two on page 146 to the diagram in Figure 1, the caption of Figure 4, and the text beginning at line 5 on page 151 stating “in our experiments the [ion] beam was 30° away from perpendicular.”

their measured yields are an order of magnitude higher than the values reported by [Sieger et al. \(1998\)](#)² for similar electron energies.

In two of our recent studies, we applied Equation 1 to our electron sputtering data and found best-fit scaling factors of $C=0.25$ ([Meier & Loeffler 2020](#)) and 0.14 ([Davis et al. 2021](#)), keeping in mind that [Meier & Loeffler \(2020\)](#) only measured Y_T and not Y_{O_2} . Following this precedent, we find the scaling factor $C=0.12$ minimizes chi-squared between $C * Y_{O_2}$ and all of our group’s data listed in Table 4. When calculating Y_{O_2} , we interpolate our electron ranges from the newly published model predicting the S_e and range of electrons in liquid H_2O by [Castillo-Rico et al. \(2021\)](#), which differs slightly from [Grün \(1957\)](#) and ESTAR ([Berger et al. 2017](#)) estimates used in [Meier & Loeffler \(2020\)](#) and [Davis et al. \(2021\)](#), and from estimates by [LaVerne & Mozumder \(1983\)](#) used by [Teolis et al. \(2010, 2017\)](#). To be consistent with the derived electron ranges in [Castillo-Rico et al. \(2021\)](#), we assume the density of H_2O -ice is the same as liquid H_2O (1 g cm^{-3}).

As seen in Figure 5, scaling Y_{O_2} down by a constant value results in a reasonable fit above 1 keV for higher temperatures, but underestimates our data at lower energies and lower temperatures, suggesting that the energy and temperature dependencies for ions are not accurately describing trends in all electron data currently available. Thus, as we now have new data for the sputtered component of O_2 , we reevaluate intrinsic parameter values ($g_{O_2}^0$, x_0 , q_0 , and Q) in Equation 1 using Markov chain Monte Carlo (MCMC) methods to determine whether we can improve the model’s overall fit while removing the need for a constant scaling factor.

5.2. Updating Parameter Values for Electrons

Here we present a brief summary of our modeling methods (see Appendix B for additional details). Due to the conflicting O_2 yields for low-energy (~ 10 to 30 eV) electrons ([Sieger et al. 1998](#); [Teolis et al. 2010](#)), we excluded both data sets from our initial MCMC analysis. However, we re-ran our MCMC optimization process using a combination of data from our group and [Sieger et al. \(1998\)](#) and from our group and [Teolis et al. \(2010\)](#). We assume an error of 100% for data from both [Sieger et al. \(1998\)](#) and [Teolis et al. \(2010\)](#).

Table 2 shows each version of our MCMC optimized values for $g_{O_2}^0$, x_0 , q_0 , and Q compared with the values determined in [Teolis et al. \(2017\)](#) for ions. Regardless of the electron data set used in the optimization, the resulting $g_{O_2}^0$ value is an order of magnitude smaller than what has been determined

Table 2. Optimized Parameter Values

Data Set	$g_{O_2}^0$ (10^{-4} eV^{-1})	x_0 (nm)	q_0	Q (eV)
Our group only	5.8 ± 3	3.6 ± 1.3	960 ± 170	0.062 ± 0.002
Our group + Sieger et al. (1998)	2.1 ± 1	10.3 ± 1.0	1090 ± 220	0.064 ± 0.002
Our group + Teolis et al. (2010)	7.4 ± 2	2.8 ± 1.0	955 ± 220	0.062 ± 0.002
Ions from Teolis et al. (2017)	50.0 ± 5	2.8 ± 0.4	1000 ± 100	0.06 ± 0.01

² The data found in the top of Figure 2 in [Orlando & Sieger \(2003\)](#) is the same as in [Sieger et al. \(1998\)](#), but there is a typo in the y-axis label of the plot (Orlando personal communication).

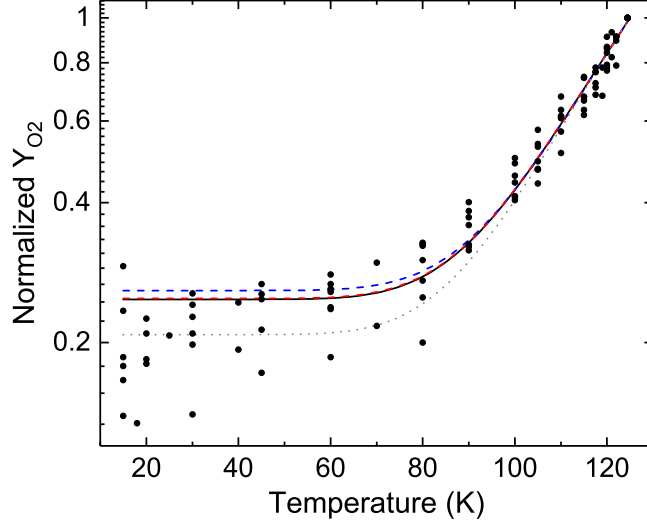


Figure 6. Equation 1 calculated using parameter values optimized to data from our group (black solid line), our group and [Sieger et al. \(1998\)](#) (blue dashed line), and our group and [Teolis et al. \(2010\)](#) (red dashed line, mostly overlapping the black solid line) normalized to unity at 124.5 K. Our group’s data for every energy normalized to unity at 124.5 K has been included (\bullet). For comparison, we also plot Equation 1 using parameter values from [Teolis et al. \(2017\)](#) for ions (grey dotted line).

for ions. Because $g_{O_2}^0$ is defined as the radiolytic yield at the surface, experimental data for lower energy (\sim eV) electrons, which do not travel very deep beneath the surface, heavily influence the optimized $g_{O_2}^0$ value. This explains the variation in $g_{O_2}^0$ values with the three electron data sets, which would likely be larger if we had stricter error for the low-energy data sets. Additionally, $g_{O_2}^0$ and x_0 are inversely correlated to each other, which explains x_0 increasing when $g_{O_2}^0$ decreases.

Our optimized values for q_0 and Q for the three data sets show less variation than did $g_{O_2}^0$ and x_0 , and all overlap with each other and with the values obtained from ions within error. As shown in Figure 6, the assumption that Y_{O_2} is approximately constant at temperatures ≤ 60 K ignores the observed weak increase in Y_{O_2} at low temperatures, which results in discrepancies between the data and model for temperatures $\lesssim 100$ K. Future modeling efforts could potentially modify the structure of Equation 1 to better fit electron data over the entire temperature range.

We plot the energy dependence of the resulting model fits and data at a single representative temperature in Figure 7, showing Y_{O_2} calculated using each set of optimized parameter values for electrons listed in Table 2 compared to $C * Y_{O_2}$ for $C=0.12$ (our best-fit scaling factor) and $C=0.29$ ([Teolis et al. 2010, 2017](#)) with Y_{O_2} calculated using parameter values for ions from [Teolis et al. \(2017\)](#). The $C=0.29$ fit used by [Teolis et al. \(2010, 2017\)](#) overestimates all of our measured O_2 sputtering rates for keV electrons. Conversely, our best fit scaling factor $C=0.12$ underestimates the yields for all of our data (with the exception of 10 keV). Equation 1 optimized to data from only our group and data combined from our group and [Teolis et al. \(2010\)](#) are very similar (and practically overlap in Figures 6 and 7), although with better constrained error for data from [Teolis et al. \(2010\)](#) differences in the resulting curves may be greater.

Finally, we note that the electron energy associated with the peak of Y_{O_2} (~ 0.65 keV) does not match the electron energy associated with the peak of electron stopping cross section (~ 0.12 keV,

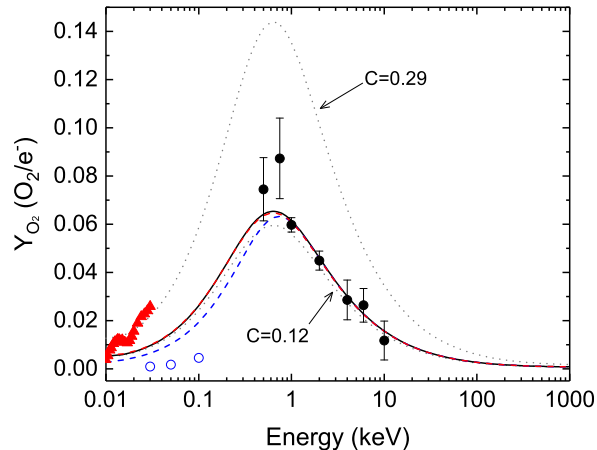


Figure 7. Modeled O_2 sputtering yields (Y_{O_2}) using Equation 1 and ion parameter values (Teolis et al. 2017) multiplied by our best fit scaling factor $C = 0.12$ (grey dotted line, labeled on plot) and $C = 0.29$ from Teolis et al. (2017) (grey dotted line, labeled on plot), and calculated with parameter values optimized using MCMC methods to match data from our group (black solid line), our group and Sieger et al. (1998) (blue dashed line), and our group and Teolis et al. (2010) (red dashed line, mostly overlapping the black solid line) for an irradiation temperature of 100 K and an electron angle of incidence of 12.5° . We also show experimental data at 100 K from our group (\bullet) and Teolis et al. (2010) (\blacktriangle), and note that the data from Sieger et al. (1998) (\circ) is at 110 K.

Castillo-Rico et al. 2021) even though Y_T is expected to trend with electron stopping cross section. Assuming the peak position of Y_{O_2} should match the peak position of Y_T , this difference could be due the overlapping Y_{O_2} values in our 0.5 and 0.75 keV data. Different models also shift the peak position of electron stopping cross section (Ashley 1982; LaVerne & Mozumder 1983; Luo et al. 1991; Gümüş 2008; Castillo-Rico et al. 2021) which could also contribute to this difference, although to a lesser extent.

6. ASTROPHYSICAL IMPLICATIONS

Below, we apply our newly optimized O_2 sputtering model for electron irradiation of H_2O -ice to three Jovian icy satellites: Europa, Ganymede, and Callisto. For Europa, we compare how the inclusion of low-energy electron experimental sputtering data affects our calculated production yields by calculating Equation 1 with each set of parameter values in Table 2. When comparing our calculations of Europa to other values in literature, and when discussing Ganymede and Callisto, we calculate Equation 1 with the parameter values optimized to our group’s data only.

6.1. Europa

As done in Davis et al. (2021), we calculate the flux of sputtered O_2 from Europa as

$$\pi \int J(E)Y_{O_2}(E, T, \beta)dE, \quad (2)$$

where $J(E)$ is the differential flux of electrons ($e^- \text{ cm}^{-2} \text{ s}^{-1} \text{ sr}^{-1} \text{ MeV}^{-1}$) near Europa, assuming a uniform electron flux striking the surface. We adopt the same differential electron flux that Davis et al.

(2021) estimated by combining measurements from the Galileo Energetic Particle Detector (Cooper 2001) and Voyager Plasma Spectrometer (Scudder et al. 1981; Sittler & Strobel 1987).

We integrate Equation 2 between 10 eV (the minimum energy required for electron sputtering; Sieger et al. 1998; Orlando & Sieger 2003) and 1 MeV, calculating Y_{O_2} with Equation 1, intrinsic parameter values from Table 2, and assuming an average β of 45°. Additionally, since Castillo-Rico et al. (2021) only calculate electron ranges up to ~430 keV, we used Castillo-Rico et al. (2021) ranges for energies ≤ 425 keV and scaled ESTAR estimated electron ranges from 425 keV to 1 MeV by a factor of 1.011 so that ranges from Castillo-Rico et al. (2021) and ESTAR matched at 425 keV.

Table 3 shows the flux of sputtered O_2 and global production rates from Europa found by scaling the sputtered flux to Europa’s surface area (mean radius from Showman & Malhotra 1999) for relevant surface temperatures (Spencer et al. 1999; Ashkenazy 2019). Interestingly, with the exception of scaling Y_{O_2} for ions down by $C=0.29$ which effectively doubles the production rate of O_2 , the choice of parameter values used to calculate the O_2 production rate does not appear to matter significantly. For instance, there is only ~5% difference between O_2 production rates at 125 K found by multiplying Y_{O_2} for ions down by $C=0.12$ (our best fit scaling factor) and calculating Y_{O_2} with parameter values found by optimizing Y_{O_2} to our group’s data. The O_2 production rates found by calculating Y_{O_2} with parameter values optimized to data from our group and Sieger et al. (1998) or data from our group and Teolis et al. (2010) differ from one another by ~17%. While a ~17% difference in the O_2 production rate for the two low-energy data sets is not seemingly large, as noted in Section 5.2, having better constrained error for the low-energy data sets would increase the difference in the resulting integrated yield. Further refining these discrepancies would require additional measurements with low-energy (~eV) electrons, which would enable a more precise estimate of the O_2 surface radiolytic yield ($g_{O_2}^0$).

While we calculated the values in Table 3 assuming a uniform electron flux striking the surface of Europa, this is an oversimplification of the radiation environment (Paranicas et al. 2001, 2009; Patterson et al. 2012; Dalton et al. 2013; Addison et al. 2023). Future studies investigating to what degree spatial variations in electron flux alter our estimates are important for properly applying our optimized electron model to Europa. Regardless, we find a global production rate of (0.5 - 1.9) $\times 10^{26}$ O_2 s^{-1} for 80 to 125 K using the parameter values optimized to our group’s data, which is slightly lower than our previous less-refined estimate (Davis et al. 2021). Additionally, our estimate

Table 3. Global Electron Sputtering from Europa.

Parameter Values Used in Equation 1	O ₂ Sputtered Flux		O ₂ Rate	
	(10 ⁸ cm ⁻² s ⁻¹)		(10 ²⁶ s ⁻¹)	
	80 K	125 K	80 K	125 K
Ion, scaled by 0.12	1.4	5.9	0.44	1.8
Ion, scaled by 0.29	3.4	14	1.1	4.4
Electron, optimized to data from our group only	1.7	6.0	0.51	1.9
Electron, optimized to data from our group + Sieger et al. (1998)	1.5	5.1	0.45	1.6
Electron, optimized to data from our group + Teolis et al. (2010)	1.7	6.1	0.52	1.9

for 125 K is a factor of ~ 1.6 times higher than the estimate made in [Vorburger & Wurz \(2018\)](#) ($1.15 \times 10^{26} \text{ O}_2 \text{ s}^{-1}$, found by multiplying the sum of the O_2 yields from both hot and cold electrons listed in their Table 5 by the surface area of Europa). Considering that, at the time of their study, the only measurement for Y_{O_2} suggested that Y_{O_2} was constant above 200 eV and about an order of magnitude higher than what we have measured at 1 keV ([Galli et al. 2017](#)), the similarity of the estimates may seem surprising. However, [Vorburger & Wurz \(2018\)](#) also assumed that only 20% of the electron flux below 1 keV reaches Europa’s surface. Recently, [Addison et al. \(2023\)](#) combined the low-energy (thermal) electron sputtering rate estimated in [Vorburger & Wurz \(2018\)](#) ($\sim 2.3 \times 10^{25} \text{ O}_2 \text{ s}^{-1}$) with a new sputtering rate estimate for 5 keV to 10 MeV electrons taking into account interactions between Jupiter’s magnetosphere and Europa’s induced magnetic field, and found the total sputtering contribution from electrons to be only $\sim 2.4 \times 10^{25} \text{ O}_2 \text{ s}^{-1}$.

While our assumption that all thermal electrons reach Europa’s surface is unlikely, it is also unlikely that there is a constant 80% reduction in flux for all electron energies below 1 keV ([Vorburger & Wurz 2018](#); [Addison et al. 2023](#)). Until there is better understanding of what portion of the lower energy ($\lesssim 5$ keV) electron flux reaches Europa’s surface, we consider our estimates to be an upper limit, as we have suggested previously based on another recent, but lower, flux estimate ([Jun et al. 2019](#)). In fact, using fluxes from [Jun et al. \(2019\)](#) results in a rate of $(1.0 - 3.7) \times 10^{25} \text{ O}_2 \text{ s}^{-1}$, which is a factor of 5 lower than our production rate, putting it in range of the value estimated by [Addison et al. \(2023\)](#). This similarity is a bit surprising, considering the estimate from [Addison et al. \(2023\)](#) is considerably more refined than ours with the inclusion of spatially resolved energetic electron fluxes, surface temperature differences, and various incident particle angles.

Our estimated range for the global electron sputtering rate of O_2 from Europa encompasses the total production rate for all ions combined of $\sim 1 \times 10^{26} \text{ O}_2 \text{ s}^{-1}$ estimated in both [Cassidy et al. \(2013\)](#) and [Addison et al. \(2021, 2022\)](#) using the unmodified Equation 1 from [Teolis et al. \(2017\)](#). While the effects of ions and electrons are unlikely to simply be additive, it is interesting that the sum of the estimate for ions and our electron estimate is similar to an estimate of O_2 production from Europa’s surface via radiation processing ($(2.2 \pm 1.2) \times 10^{26} \text{ O}_2 \text{ s}^{-1}$), which was extrapolated from measurements of atmospheric H_2 loss rates during Juno’s recent fly-by of Europa ([Szalay et al. 2024](#)). Considering the possible reduction of our electron sputtering rate estimates from the deflection of thermal electrons near Europa and that we also recently found Equation 1 likely overestimates Y_{O_2} by a factor of 5 to 8 at 120 K for 0.5 to 5 keV ions ([Tribbett & Loeffler 2021](#)), which are representative of the cold/thermal ion component near Europa, more rigorous investigation is needed to determine whether the apparent agreement with the Juno-derived data is fortuitous. Nonetheless, we expect that, at the very least, electrons are significant contributors to the sputter-produced O_2 exosphere around Europa and need to be considered in any future modeling efforts.

6.2. *Ganymede*

Ganymede has an exosphere predominately composed of O_2 , atomic O, and H_2O ([Hall et al. 1998](#); [De Kleer et al. 2023](#)) hypothesized to be produced via sputtering and sublimation. Sputtering from Ganymede by Jupiter’s magnetospheric particles is complicated by Ganymede’s intrinsic magnetic field deflecting certain energetic particles away from the moon’s surface ([Delitsky & Lane 1998](#); [Plainaki 2015](#); [Fatemi et al. 2016](#); [Poppe et al. 2018](#); [Liuzzo et al. 2020](#)). A recent study ([Liuzzo et al. 2020](#)) showed Ganymede’s closed field lines around its equator completely shield the moon’s equato-

rial region from irradiating electrons with energies $\lesssim 40$ MeV, while electrons of all energies reach the surface of Ganymede’s polar regions (Frank et al. 1997; Cooper 2001; Liuzzo et al. 2020).

We estimate the flux of O_2 sputtered from Ganymede by electrons with Equation 2, calculating Y_{O_2} with Equation 1, parameter values optimized to our group’s data, and assuming $J(E)$ for electrons near Ganymede’s orbital radius (Paranicas et al. 2021) contributes to a uniform electron flux striking Ganymede’s polar regions. We extrapolate the differential electron fluxes given in Paranicas et al. (2021) down to 10 eV in order to integrate from 10 eV to 1 MeV. We find the flux of sputtered O_2 to be $(3 - 20) \times 10^7 \text{ cm}^{-2} \text{ s}^{-1}$ for 65 to 140 K (limits for the temperature range at Ganymede’s poles; Squyres 1980). Using the mean radius for Ganymede (Showman & Malhotra 1999) and scaling our O_2 sputtered flux estimate by the area of the polar regions where electrons reach the surface (latitudes $\geq 40^\circ$; Liuzzo et al. 2020) yields a production rate of $(0.9 - 6.2) \times 10^{25} \text{ O}_2 \text{ s}^{-1}$ for 65 to 140 K, which, to our knowledge, is the first estimate for O_2 production rates from Ganymede by irradiating electrons. While our estimate could be refined further, it appears to be significantly lower than the most recent estimate for O_2 production by ions of $2.4 \times 10^{26} \text{ O}_2 \text{ s}^{-1}$ by Pontoni et al. (2022), and even lower than earlier estimates for ions by Marconi (2007) ($1.2 \times 10^{27} \text{ O}_2 \text{ s}^{-1}$) and Plainaki (2015) ($2.6 \times 10^{28} \text{ O}_2 \text{ s}^{-1}$). However, given that Pontoni et al. (2022) used Equation 1 and found that low-energy ($\sim \text{keV}$) ions were the major contributor to the O_2 sputtering flux, it is possible that the production rates for ions were overestimated (see above). Regardless, given the simplicity of our estimate, as well as the wide range of estimates for sputtering from ions, more studies investigating sputtering from Ganymede’s surface may be merited.

6.3. Callisto

O_2 has also been detected in Callisto’s atmosphere (Cunningham et al. 2015; De Kleer et al. 2023). While sputtering has been speculated to play a key role for decades (Kliore et al. 2002), surface particle fluxes are difficult to assess due to the presence of Callisto’s atmosphere (Strobel et al. 2002). Recently, Carberry Mogan et al. (2023) modeled the spatial variation in temperature and particle (electron and hydrogen, oxygen, and sulfur ion) fluxes across the surface of Callisto. They then calculated sputtering rates for ions using both the model developed by Famá et al. (2008) and modified by Johnson et al. (2009) as well Equation 1 (Teolis et al. 2017) with parameter values for ions modified in Tribbett & Loeffler (2021), and for electrons using Equation 1 with parameter values derived for ions (Teolis et al. 2017) and no scaling factor. They determine that, although sputtering from Callisto’s surface is not enough to account for the observed column densities of O_2 in Callisto’s atmosphere, electrons contribute between 24 to 32% of the total O_2 sputtered from Callisto’s icy patches, which is more than the contribution from hydrogen (~ 0.5 to 7%) and oxygen (18 to 20%) ions, but less than from sulfur ions (57 to 41%).

While recalculating the spatially resolved sputtering yields from Callisto’s ice patches is beyond the scope of this work, here we estimate the effect that our new electron parameter values have on the predicted O_2 sputtered from Callisto’s surface. Although we cannot use Equation 2, due to the complication of the impinging flux interacting with the moon’s atmosphere, we make a rough estimate by integrating the radiolytic yield ($G_{O_2} = Y_{O_2}/E$) at temperatures relevant for Callisto (80 to 144 K; Grundy 1999; Carberry Mogan et al. 2023) with our new electron parameter values and compare that result with what we obtain when we perform the integration with the parameters values used in Carberry Mogan et al. (2023). Integrating from 10 eV to 1 MeV, we find that our new electron parameter values reduce the yield by an order magnitude, suggesting that the contribution of electrons

to sputtering of O₂ from Callisto is likely significantly less than as estimated by Carberry Mogan et al. (2023).

7. CONCLUSIONS

In this paper, we measured the total, H₂O, and O₂ sputtering yields for electrons with energies between 0.75 and 10 keV and for irradiation temperatures between 15 and 124.5 K. Over our studied energies, we found that both total and O₂ yields increase with decreasing energy (increasing S_e) and increase rapidly at temperatures above 60 K, which is in agreement with our previous electron work, as well as previous studies with electrons and ions. In addition, we find that the yield of H₂O has a nearly quadratic relation with S_e while the yield of O₂ appears to trend approximately linearly with S_e (although the slope changes with temperature). These different dependencies could explain why the trend of Y_T with S_e ranges from quadratic to linear in previous studies for light ions and electrons. Additionally, the composition of the sputtered flux has a strong dependence on electron energy with the relative amount of H₂O decreasing rapidly with decreasing S_e over the electron energies studied. In fact, we find that above 4 keV, the contribution from H₂O is essentially zero within the limits of our error.

Combining our data with O₂ sputtering yields for 0.5 keV electrons from Davis et al. (2021) and other low-energy (~eV) electron data from literature (Sieger et al. 1998; Teolis et al. 2010), we reevaluated intrinsic parameters in the sputtering model from Teolis et al. (2017), finding that we can provide a more satisfying fit while also removing the arbitrary scaling factor. Having better constraints on low-energy electron O₂ yields in literature or restructuring the energy and/or temperature dependent model components may improve the fit further.

Combining our newly optimized sputtering model with incoming electron fluxes near Europa, we calculate that electrons may contribute to the production of Europa's O₂ exosphere at a rate similar to all ion types combined. Thus, although electrons may, in most cases, have significantly lower individual sputtering yields than ions, the higher electron fluxes at the surface of icy bodies like Europa may be large enough for electrons to be a major contributor to exospheric O₂ production. In contrast, we find electrons contribute less to O₂ sputtering from Ganymede and Callisto, although the contribution of electrons is still likely non-negligible. Of course, future studies for all moons examining spatial variations in the incoming electron flux are needed to refine our estimates. Regardless, at the very least, it seems clear that the contribution of electrons needs to be included in sputtering and exosphere modeling of icy bodies going forward.

We would like to thank T.M. Orlando and B.D. Teolis for explaining their group's published electron sputtering data as well as P.D. Tribbett for contributing to the MCMC methods discussion. This research was supported by NASA Solar System Workings Award #80NSSC20K0464. Data can be found in Northern Arizona University's long-term repository <https://openknowledge.nau.edu/id/eprint/6258>).

APPENDIX

A. DATA

In Table 4, we list our measured total, H₂O, and O₂ sputtering yields for each electron energy and temperature studied in this paper and in [Davis et al. \(2021\)](#). Molecular H₂ sputtering yields are calculated as $Y_{H_2} = 2 * Y_{O_2}$.

Table 4. All Laboratory Sputtering Yields

Temperature (K)	Total Yield (10 ⁻²⁴ g/e ⁻)	H ₂ O Yield (H ₂ O/e ⁻)	O ₂ Yield ^a (O ₂ /e ⁻)
0.5 keV electrons^b			
15	6.62	0.17	0.025
30	6.63	0.17	0.025
45	6.98	0.17	0.031
60	7.13	0.17	0.034
80	7.83	0.17	0.045
90	8.60	0.17	0.058
100	9.57	0.17	0.075
105	10.23	0.17	0.086
110	11.77	0.17	0.111
115	12.31	0.17	0.120
117.5	13.58	0.17	0.142
120	13.56	0.17	0.141
122	14.80	0.17	0.162
124.5	15.94	0.17	0.181
0.75 keV electrons			
15	5.32	0.094	0.042
20	5.05	0.094	0.038
30	5.39	0.094	0.043
45	5.46	0.094	0.045
60	5.57	0.094	0.046
80	6.29	0.094	0.058
90	7.19	0.094	0.072
100	8.02	0.094	0.087
105	8.97	0.094	0.103
110	9.62	0.094	0.114

Table 4 continued on next page

Table 4 (*continued*)

Temperature (K)	Total Yield (10^{-24} g/e $^{-}$)	H₂O Yield (H ₂ O/e $^{-}$)	O₂ Yield^a (O ₂ /e $^{-}$)
115	10.79	0.094	0.134
117.5	11.03	0.094	0.138
120	11.84	0.094	0.151
122	12.61	0.094	0.164
124.5	13.55	0.094	0.180
1 keV electrons			
15	3.54	0.068	0.025
20	3.53	0.068	0.025
30	3.74	0.068	0.027
45	4.19	0.068	0.036
60	3.96	0.068	0.032
80	4.46	0.068	0.041
90	5.04	0.068	0.050
100	5.61	0.068	0.060
105	6.30	0.068	0.071
110	6.63	0.068	0.077
115	7.49	0.068	0.091
117.5	7.87	0.068	0.098
120	8.44	0.068	0.107
122	9.39	0.068	0.123
124.5	10.11	0.068	0.135
2 keV electrons			
15	2.05	0.016	0.026
30	1.86	0.016	0.023
40	1.79	0.016	0.022
60	1.99	0.016	0.025
70	2.08	0.016	0.027
80	2.22	0.016	0.029
90	2.55	0.016	0.035
100	3.17	0.016	0.045
105	3.36	0.016	0.048
110	3.75	0.016	0.055

Table 4 *continued on next page*

Table 4 (*continued*)

Temperature (K)	Total Yield (10^{-24} g/e $^{-}$)	H₂O Yield (H ₂ O/e $^{-}$)	O₂ Yield^a (O ₂ /e $^{-}$)
115	4.50	0.016	0.067
120	5.10	0.016	0.077
124.5	5.86	0.016	0.090
4 keV electrons			
15	0.93	0.006	0.013
18	0.74	0.006	0.009
25	1.05	0.006	0.015
30	1.06	0.006	0.015
45	1.08	0.006	0.015
60	1.17	0.006	0.017
80	1.32	0.006	0.019
90	1.69	0.006	0.025
100	1.89	0.006	0.029
105	2.03	0.006	0.031
110	2.34	0.006	0.036
115	2.79	0.006	0.044
117.5	3.06	0.006	0.048
119	3.04	0.006	0.048
120	3.42	0.006	0.054
121	3.65	0.006	0.058
122	3.51	0.006	0.056
124.5	4.40	0.006	0.071
6 keV electrons			
15	0.57	0	0.010
20	0.62	0	0.010
30	0.78	0	0.013
45	0.88	0	0.015
60	0.90	0	0.015
80	1.13	0	0.019
90	1.12	0	0.019
100	1.58	0	0.026
105	1.62	0	0.027

Table 4 *continued on next page*

Table 4 (*continued*)

Temperature (K)	Total	H ₂ O	O ₂
	Yield (10 ⁻²⁴ g/e ⁻)	Yield (H ₂ O/e ⁻)	Yield ^a (O ₂ /e ⁻)
110	2.12	0	0.035
115	2.33	0	0.039
120	2.99	0	0.050
122	3.15	0	0.053
124.5	3.45	0	0.058
10 keV electrons			
20	0.50	0.004	0.006
40	0.45	0.004	0.005
60	0.58	0.004	0.008
70	0.49	0.004	0.006
80	0.46	0.004	0.006
90	0.66	0.004	0.009
100	0.82	0.004	0.012
105	0.96	0.004	0.014
110	1.27	0.004	0.019
115	1.20	0.004	0.018
117.5	1.42	0.004	0.022
119	1.45	0.004	0.022
120	1.67	0.004	0.026
121	1.71	0.004	0.026
124.5	1.82	0.004	0.028

^amolecular yield of H₂ is twice that of O₂ ($Y_{H_2} = 2 * Y_{O_2}$)

^bfrom [Davis et al. \(2021\)](#)

B. MODEL OPTIMIZATION

To determine the values of $g_{O_2}^0$, x_0 , q_0 and Q in Equation 1, [Teolis et al. \(2010, 2017\)](#) split the equation into separate energy and temperature dependencies. They fit the temperature-independent data (≤ 80 K) to the energy-dependent component to determine $g_{O_2}^0$ and x_0 and then found q_0 and Q by fitting the temperature-dependent component to O₂ yields for all energies normalized to unity at 150 K. Our use of MCMC methods to optimize the model to electron data enables us to determine values for all parameters ($g_{O_2}^0$, x_0 , q_0 , and Q) without splitting Equation 1 into energy and temperature

components. This allows us to optimize the model to every data point available regardless of energy or temperature.

We use “emcee,” an open-source software package in Python (Foreman-Mackey et al. 2013) to optimize Equation 1 from Teolis et al. (2017) to electron laboratory data. While more commonly used for observational astronomy (Dunkley et al. 2005; Line et al. 2015; Tribbett et al. 2021; and many others), our group has previously used emcee to match existing models/equations to experimental data (Behr et al. 2020; Carmack et al. 2023).

Briefly, emcee uses Markov chain Monte Carlo (MCMC) methods with Bayesian inference (as described in Foreman-Mackey et al. 2013 and Behr et al. 2020) in order to explore the probability distribution of parameters in a model when compared to an observed data set. It does this by utilizing “walkers” which move around the model’s multi-dimensional parameter space along a Markov chain. Each “step” in the Markov chain, or change in parameter values, depends only on how the probability of the current walker values compare to a random sampling of possible new values. With enough steps in the chain, MCMC forgets the user-specified initial parameter values and is able to escape local solutions. Moreover, no additional knowledge (other than defining the likelihood function) is needed to run emcee, eliminating the constraints of grid searches such as user defined spacing/resolution and limiting values. Furthermore, while the points in a grid search scale exponentially with dimensionality, this is not necessarily the case with MCMC, potentially making computational times with MCMC faster. This puts MCMC above other commonly used fitting methods (e.g. by eye or using a grid method, see Speagle 2019 for more details) by thoroughly exploring the probability of observed data being described by the model throughout the multi-dimensional parameter space.

We gave all parameters ($g_{O_2}^0$, x_0 , q_0 , and Q) flat priors limiting them to physical values (i.e. ≥ 0), and we gave x_0 an additional Gaussian prior of 5 ± 4 nm in order to encompass estimates of efficient O_2 production depths from Petrik et al. (2006) and Meier & Loeffler (2020). Walkers in MCMC can and will stray away from the mean of the specified Gaussian prior if the likelihood of the observed data given the model prefers it. We randomly distributed initial parameter values for walkers around an estimate made by fitting Equation 1 to the data by eye. While not necessary, starting walkers with an educated guess will reduce the number of steps and therefore computational time the walkers need in order to constrain the posterior distribution and best fit parameter values (unless of course the educated guess was a poor one or a local solution).

We ran our MCMC optimization process with three Y_{O_2} data sets: from our group, from our group and Sieger et al. (1998), and from our group and Teolis et al. (2010). We modeled the data from Sieger et al. (1998) and Teolis et al. (2010) separately because of their large differences in Y_{O_2} for similar electron energies (see Figure 7). We scaled their data by $\cos^{1.3}(\beta)/\cos^{1.3}(12.5^\circ)$ (Vidal et al. 2005) to account for the differences in incidence angle (β) and assumed 100% error for data from both Sieger et al. (1998) and Teolis et al. (2010) due to no error being provided in the original manuscripts and due to possible differences in sample thickness affecting the reported sputtering yields (Petrik & Kimmel 2005). Like we did for our own data, we interpolated electron ranges from Castillo-Rico et al. (2021) for the relevant electron energies used by Sieger et al. (1998) and Teolis et al. (2010). We list the optimized values for $g_{O_2}^0$, x_0 , q_0 , and Q for all data sets in Table 2 and provide additional discussion in Section 5.2.

REFERENCES

- | | |
|---|---|
| <p>Abdulgalil, A. G. M., Rosu-Finsen, A., Marchione, D., et al. 2017, ACS Earth and Space Chemistry, 1, 209, doi: 10.1021/acsearthspacechem.7b00028</p> | <p>Addison, P., Liuzzo, L., Arnold, H., & Simon, S. 2021, Journal of Geophysical Research: Space Physics, 126, e2020JA029087, doi: 10.1029/2020JA029087</p> |
|---|---|

- Addison, P., Liuzzo, L., & Simon, S. 2022, *Journal of Geophysical Research: Space Physics*, 127, e2021JA030136, doi: [10.1029/2021JA030136](https://doi.org/10.1029/2021JA030136)
- . 2023, *Journal of Geophysical Research: Space Physics*, 128, e2023JA031734, doi: [10.1029/2023JA031734](https://doi.org/10.1029/2023JA031734)
- Ashkenazy, Y. 2019, *Heliyon*, 5, e01908, doi: [10.1016/j.heliyon.2019.e01908](https://doi.org/10.1016/j.heliyon.2019.e01908)
- Ashley, J. 1982, *Journal of Electron Spectroscopy and Related Phenomena*, 28, 177, doi: [10.1016/0368-2048\(82\)85041-X](https://doi.org/10.1016/0368-2048(82)85041-X)
- Bar-Nun, A., Herman, G., Rappaport, M., & Mekler, Y. 1985, *Surface Science*, 150, 143, doi: [10.1016/0039-6028\(85\)90215-8](https://doi.org/10.1016/0039-6028(85)90215-8)
- Baragiola, R., Atteberry, C., Dukes, C., Famá, M., & Teolis, B. 2002, *Nuclear Instruments and Methods in Physics Research Section B: Beam Interactions with Materials and Atoms*, 193, 720, doi: [10.1016/S0168-583X\(02\)00893-5](https://doi.org/10.1016/S0168-583X(02)00893-5)
- Baragiola, R., Vidal, R., Svendsen, W., et al. 2003, *Nuclear Instruments and Methods in Physics Research Section B: Beam Interactions with Materials and Atoms*, 209, 294, doi: [10.1016/S0168-583X\(02\)02052-9](https://doi.org/10.1016/S0168-583X(02)02052-9)
- Behr, P. R., Tribbett, P. D., Robinson, T. D., & Loeffler, M. J. 2020, *The Astrophysical Journal*, 900, 147, doi: [10.3847/1538-4357/abad3f](https://doi.org/10.3847/1538-4357/abad3f)
- Berger, M. J., Coursey, J. S., Zucker, M. A., & Chang, J. 2017, *ESTAR, PSTAR, and ASTAR: Computer Programs for Calculating Stopping-Power and Range Tables for Electrons, Protons, and Helium Ions*, National Institute of Standards and Technology, doi: [10.18434/T4NC7P](https://doi.org/10.18434/T4NC7P)
- Boring, J., Johnson, R., Reimann, C., et al. 1983, *Nuclear Instruments and Methods in Physics Research*, 218, 707, doi: [10.1016/0167-5087\(83\)91070-0](https://doi.org/10.1016/0167-5087(83)91070-0)
- Brown, W., Augustyniak, W., Brody, E., et al. 1980a, *Nuclear Instruments and Methods*, 170, 321, doi: [10.1016/0029-554X\(80\)91033-2](https://doi.org/10.1016/0029-554X(80)91033-2)
- Brown, W., Augustyniak, W., Lanzerotti, L., Johnson, R., & Evatt, R. 1980b, *Physical Review Letters*, 45, 1632, doi: [10.1103/PhysRevLett.45.1632](https://doi.org/10.1103/PhysRevLett.45.1632)
- Brown, W., Augustyniak, W., Marcantonio, K., et al. 1984, *Nuclear Instruments and Methods in Physics Research Section B: Beam Interactions with Materials and Atoms*, 1, 307, doi: [10.1016/0168-583X\(84\)90085-5](https://doi.org/10.1016/0168-583X(84)90085-5)
- Carberry Mogan, S. R., Liuzzo, L., Poppe, A. R., et al. 2023, *Journal of Geophysical Research: Planets*, 128, doi: [10.1029/2023JE007894](https://doi.org/10.1029/2023JE007894)
- Carmack, R. A., Tribbett, P. D., & Loeffler, M. J. 2023, *The Astrophysical Journal*, 942, 1, doi: [10.3847/1538-4357/aca76b](https://doi.org/10.3847/1538-4357/aca76b)
- Carnielli, G., Galand, M., Leblanc, F., et al. 2020, *Icarus*, 351, 113918, doi: [10.1016/j.icarus.2020.113918](https://doi.org/10.1016/j.icarus.2020.113918)
- Cassidy, T., Paranicas, C., Shirley, J., et al. 2013, *Planetary and Space Science*, 77, 64, doi: [10.1016/j.pss.2012.07.008](https://doi.org/10.1016/j.pss.2012.07.008)
- Castillo-Rico, L., Flores-Mancera, M., & Massillon-JL, G. 2021, *Nuclear Instruments and Methods in Physics Research Section B: Beam Interactions with Materials and Atoms*, 502, 189, doi: [10.1016/j.nimb.2021.07.002](https://doi.org/10.1016/j.nimb.2021.07.002)
- Cooper, J. 2001, *Icarus*, 149, 133, doi: [10.1006/icar.2000.6498](https://doi.org/10.1006/icar.2000.6498)
- Cunningham, N. J., Spencer, J. R., Feldman, P. D., et al. 2015, *Icarus*, 254, 178, doi: [10.1016/j.icarus.2015.03.021](https://doi.org/10.1016/j.icarus.2015.03.021)
- Dalton, J., Cassidy, T., Paranicas, C., et al. 2013, *Planetary and Space Science*, 77, 45, doi: [10.1016/j.pss.2012.05.013](https://doi.org/10.1016/j.pss.2012.05.013)
- Davis, M. R., Meier, R. M., Cooper, J. F., & Loeffler, M. J. 2021, *The Astrophysical Journal Letters*, 908, L53, doi: [10.3847/2041-8213/abe415](https://doi.org/10.3847/2041-8213/abe415)
- De Kleer, K., Milby, Z., Schmidt, C., Camarca, M., & Brown, M. E. 2023, *The Planetary Science Journal*, 4, 37, doi: [10.3847/PSJ/acb53c](https://doi.org/10.3847/PSJ/acb53c)
- Delitsky, M. L., & Lane, A. L. 1998, *Journal of Geophysical Research*, 103, 31391, doi: [https://doi.org/10.1029/1998JE900020](https://doi.org/https://doi.org/10.1029/1998JE900020)
- Dunkley, J., Bucher, M., Ferreira, P. G., Moodley, K., & Skordis, C. 2005, *Monthly Notices of the Royal Astronomical Society*, 356, 925, doi: [10.1111/j.1365-2966.2004.08464.x](https://doi.org/10.1111/j.1365-2966.2004.08464.x)
- Famá, M., Shi, J., & Baragiola, R. 2008, *Surface Science*, 602, 156, doi: [10.1016/j.susc.2007.10.002](https://doi.org/10.1016/j.susc.2007.10.002)
- Fatemi, S., Poppe, A. R., Khurana, K. K., Holmström, M., & Delory, G. T. 2016, *Geophysical Research Letters*, 43, 4745, doi: [10.1002/2016GL068363](https://doi.org/10.1002/2016GL068363)
- Foreman-Mackey, D., Hogg, D. W., Lang, D., & Goodman, J. 2013, *Publications of the Astronomical Society of the Pacific*, 125, 306, doi: [10.1086/670067](https://doi.org/10.1086/670067)

- Frank, L. A., Paterson, W. R., Ackerson, K. L., & Bolton, S. J. 1997, *Geophysical Research Letters*, 24, 2159, doi: [10.1029/97GL01632](https://doi.org/10.1029/97GL01632)
- Galli, A., Vorburgeter, A., Wurcz, P., & Tulej, M. 2017, *Icarus*, 291, 36, doi: [10.1016/j.icarus.2017.03.018](https://doi.org/10.1016/j.icarus.2017.03.018)
- Galli, A., Vorburgeter, A., Wurcz, P., et al. 2018, *Planetary and Space Science*, 155, 91, doi: [10.1016/j.pss.2017.11.016](https://doi.org/10.1016/j.pss.2017.11.016)
- Gamborino, D., Vorburgeter, A., & Wurcz, P. 2019, *Annales Geophysicae*, 37, 455, doi: [10.5194/angeo-37-455-2019](https://doi.org/10.5194/angeo-37-455-2019)
- Grundy, W. 1999, *Icarus*, 142, 536, doi: [10.1006/icar.1999.6216](https://doi.org/10.1006/icar.1999.6216)
- Grün, A. E. 1957, *Zeitschrift für Naturforschung A*, 12, 89, doi: [10.1515/zna-1957-0201](https://doi.org/10.1515/zna-1957-0201)
- Gümüş, H. 2008, *Applied Radiation and Isotopes*, 66, 1886
- Hall, D. T., Feldman, P. D., McGrath, M. A., & Strobel, D. F. 1998, *The Astrophysical Journal*, 499, 475, doi: [10.1086/305604](https://doi.org/10.1086/305604)
- Hall, D. T., Strobel, D. F., Feldman, P. D., McGrath, M. A., & Weaver, H. A. 1995, *Nature*, 373, 677, doi: [10.1038/373677a0](https://doi.org/10.1038/373677a0)
- Heide, H.-G. 1984, *Ultramicroscopy*, 14, 271, doi: [10.1016/0304-3991\(84\)90095-0](https://doi.org/10.1016/0304-3991(84)90095-0)
- Ip, W., Williams, D. J., McEntire, R. W., & Mauk, B. 1997, *Geophysical Research Letters*, 24, 2631, doi: [10.1029/97GL02814](https://doi.org/10.1029/97GL02814)
- Johnson, R., Lanzerotti, L., & Brown, W. 1982, *Nuclear Instruments and Methods in Physics Research*, 198, 147, doi: [10.1016/0167-5087\(82\)90066-7](https://doi.org/10.1016/0167-5087(82)90066-7)
- Johnson, R. E., Burger, M. H., Cassidy, T. A., et al. 2009, *Composition and Detection of Europa's Sputter-induced Atmosphere* (University of Arizona Press), 507–528. <http://www.jstor.org/stable/j.ctt1xp3wdw.27>
- Jun, I., Garrett, H. B., Cassidy, T. A., Kim, W., & Dougherty, L. 2019, *IEEE Transactions on Plasma Science*, 47, 3915, doi: [10.1109/TPS.2019.2901681](https://doi.org/10.1109/TPS.2019.2901681)
- Kliore, A. J., Anabtawi, A., Herrera, R. G., et al. 2002, *Journal of Geophysical Research: Space Physics*, 107, doi: [10.1029/2002JA009365](https://doi.org/10.1029/2002JA009365)
- LaVerne, J. A., & Mozumder, A. 1983, *Radiation Research*, 96, 219, doi: [10.2307/3576206](https://doi.org/10.2307/3576206)
- Ligier, N., Paranicas, C., Carter, J., et al. 2019, *Icarus*, 333, 496, doi: [10.1016/j.icarus.2019.06.013](https://doi.org/10.1016/j.icarus.2019.06.013)
- Line, M. R., Teske, J., Burningham, B., Fortney, J. J., & Marley, M. S. 2015, *The Astrophysical Journal*, 807, 183, doi: [10.1088/0004-637X/807/2/183](https://doi.org/10.1088/0004-637X/807/2/183)
- Liuzzo, L., Poppe, A. R., Paranicas, C., et al. 2020, *Journal of Geophysical Research: Space Physics*, 125, e2020JA028347, doi: [10.1029/2020JA028347](https://doi.org/10.1029/2020JA028347)
- Luo, S., Zhang, X., & Joy, D. C. 1991, *Radiation Effects and Defects in Solids*, 117, 235, doi: [10.1080/10420159108220619](https://doi.org/10.1080/10420159108220619)
- Marconi, M. 2007, *Icarus*, 190, 155, doi: [10.1016/j.icarus.2007.02.016](https://doi.org/10.1016/j.icarus.2007.02.016)
- Meier, R. M., & Loeffler, M. J. 2020, *Surface Science*, 691, 121509, doi: [10.1016/j.susc.2019.121509](https://doi.org/10.1016/j.susc.2019.121509)
- Orlando, T., & Sieger, M. 2003, *Surface Science*, 528, 1, doi: [10.1016/S0039-6028\(02\)02602-X](https://doi.org/10.1016/S0039-6028(02)02602-X)
- Paranicas, C., Carlson, R. W., & Johnson, R. E. 2001, *Geophysical Research Letters*, 28, 673, doi: [10.1029/2000GL012320](https://doi.org/10.1029/2000GL012320)
- Paranicas, C., Cooper, J. F., Garrett, H. B., et al. 2009, *Europa's Radiation Environment and Its Effects on the Surface* (University of Arizona Press), 529–544. <http://www.jstor.org/stable/j.ctt1xp3wdw.28>
- Paranicas, C., Szalay, J. R., Mauk, B. H., et al. 2021, *Geophysical Research Letters*, 48, e2021GL093021, doi: [10.1029/2021GL093021](https://doi.org/10.1029/2021GL093021)
- Paranicas, C., Mauk, B. H., Kollmann, P., et al. 2022, *Geophysical Research Letters*, 49, e2022GL098077, doi: [10.1029/2022GL098077](https://doi.org/10.1029/2022GL098077)
- Patterson, G. W., Paranicas, C., & Prockter, L. M. 2012, *Icarus*, 220, 286, doi: [10.1016/j.icarus.2012.04.024](https://doi.org/10.1016/j.icarus.2012.04.024)
- Petrik, N. G., Kavetsky, A. G., & Kimmel, G. A. 2006, *The Journal of Physical Chemistry B*, 110, 2723, doi: [10.1021/jp055173v](https://doi.org/10.1021/jp055173v)
- Petrik, N. G., & Kimmel, G. A. 2005, *The Journal of Chemical Physics*, 123, 054702, doi: [10.1063/1.1943388](https://doi.org/10.1063/1.1943388)
- Plainaki, C. 2015, *Icarus*, 245, 306, doi: [10.1016/j.icarus.2014.09.018](https://doi.org/10.1016/j.icarus.2014.09.018)
- Plainaki, C., Massetti, S., Jia, X., et al. 2020, *The Astrophysical Journal*, 900, 74, doi: [10.3847/1538-4357/aba94c](https://doi.org/10.3847/1538-4357/aba94c)
- Pontoni, A., Shimoyama, M., Futaana, Y., et al. 2022, *Journal of Geophysical Research: Space Physics*, 127, e2021JA029439, doi: [10.1029/2021JA029439](https://doi.org/10.1029/2021JA029439)

- Poppe, A. R., Fatemi, S., & Khurana, K. K. 2018, *Journal of Geophysical Research: Space Physics*, 123, 4614, doi: [10.1029/2018JA025312](https://doi.org/10.1029/2018JA025312)
- Sack, N. J., & Baragiola, R. A. 1993, *Physical Review B*, 48, 9973, doi: [10.1103/PhysRevB.48.9973](https://doi.org/10.1103/PhysRevB.48.9973)
- Scudder, J. D., Sittler, E. C., & Bridge, H. S. 1981, *Journal of Geophysical Research: Space Physics*, 86, 8157, doi: [10.1029/JA086iA10p08157](https://doi.org/10.1029/JA086iA10p08157)
- Shi, M., Baragiola, R. A., Grosjean, D. E., et al. 1995, *Journal of Geophysical Research*, 100, 26387, doi: [10.1029/95JE03099](https://doi.org/10.1029/95JE03099)
- Showman, A. P., & Malhotra, A. R. 1999, *Science*, 286, 77, doi: [10.1126/science.286.5437.77](https://doi.org/10.1126/science.286.5437.77)
- Sieger, M. T., Simpson, W. C., & Orlando, T. M. 1998, *Nature*, 394, 554, doi: [10.1038/29015](https://doi.org/10.1038/29015)
- Sittler, E. C., & Strobel, D. F. 1987, *Journal of Geophysical Research: Space Physics*, 92, 5741, doi: [10.1029/JA092iA06p05741](https://doi.org/10.1029/JA092iA06p05741)
- Speagle, J. S. 2019, doi: [10.48550/ARXIV.1909.12313](https://doi.org/10.48550/ARXIV.1909.12313)
- Spencer, J. R., Tamppari, L. K., Martin, T. Z., & Travis, L. D. 1999, *Science*, 284, 1514, doi: [10.1126/science.284.5419.1514](https://doi.org/10.1126/science.284.5419.1514)
- Squyres, S. W. 1980, *Icarus*, 44, 502, doi: [10.1016/0019-1035\(80\)90040-8](https://doi.org/10.1016/0019-1035(80)90040-8)
- Stern, S. A. 1999, *Reviews of Geophysics*, 37, 453, doi: [10.1029/1999RG900005](https://doi.org/10.1029/1999RG900005)
- Strobel, D. F., Saur, J., Feldman, P. D., & McGrath, M. A. 2002, *The Astrophysical Journal*, 581, L51, doi: [10.1086/345803](https://doi.org/10.1086/345803)
- Szalay, J. R., Allegrini, F., Ebert, R. W., et al. 2024, *Nature Astronomy*, doi: [10.1038/s41550-024-02206-x](https://doi.org/10.1038/s41550-024-02206-x)
- Teolis, B. D., Plainaki, C., Cassidy, T. A., & Raut, U. 2017, *Journal of Geophysical Research: Planets*, 122, 1996, doi: [10.1002/2017JE005285](https://doi.org/10.1002/2017JE005285)
- Teolis, B. D., Shi, J., & Baragiola, R. A. 2009, *The Journal of Chemical Physics*, 130, 134704, doi: [10.1063/1.3091998](https://doi.org/10.1063/1.3091998)
- Teolis, B. D., Vidal, R. A., Shi, J., & Baragiola, R. A. 2005, *Physical Review B*, 72, 245422, doi: [10.1103/PhysRevB.72.245422](https://doi.org/10.1103/PhysRevB.72.245422)
- Teolis, B. D., Jones, G. H., Miles, P. F., et al. 2010, *Science*, 330, 1813, doi: [10.1126/science.1198366](https://doi.org/10.1126/science.1198366)
- Tribbett, P. D., & Loeffler, M. J. 2021, *Surface Science*, 707, 121797, doi: [10.1016/j.susc.2021.121797](https://doi.org/10.1016/j.susc.2021.121797)
- Tribbett, P. D., Robinson, T. D., & Koskinen, T. T. 2021, *The Planetary Science Journal*, 2, 109, doi: [10.3847/PSJ/abf92d](https://doi.org/10.3847/PSJ/abf92d)
- Vidal, R., Teolis, B., & Baragiola, R. 2005, *Surface Science*, 588, 1, doi: [10.1016/j.susc.2005.05.007](https://doi.org/10.1016/j.susc.2005.05.007)
- Vorburger, A., & Wurz, P. 2018, *Icarus*, 311, 135, doi: [10.1016/j.icarus.2018.03.022](https://doi.org/10.1016/j.icarus.2018.03.022)
- Wurz, P., Rohner, U., Whitby, J., et al. 2007, *Icarus*, 191, 486, doi: [10.1016/j.icarus.2007.04.034](https://doi.org/10.1016/j.icarus.2007.04.034)
- Wurz, P., Whitby, J., Rohner, U., et al. 2010, *Planetary and Space Science*, 58, 1599, doi: [10.1016/j.pss.2010.08.003](https://doi.org/10.1016/j.pss.2010.08.003)